Energy Management of Stand-Alone Rural Micro-Grid Application based PV – Batteries–System in Guinea

Mohamed Lamine Touré[1,2], Mamadou-Baïlo Camara[1,2,3], Fahad Maoulida[1], Alireza Payman[1], and Brayima Dakyo[1]

[1] GREAH Laboratory, University of Le Havre Normandie, 75 Rue Bellot, 76600 Le Havre, France
[2] Laboratoire d'Enseignement et de Recherche en Énergétique et Automatique (LENA), Université Gamal Abdel Nasser Conakry, Guinea
[3] Laboratoire de Recherche en Sciences Appliquées de Mamou (LaReSA), Institut Supérieur de Technologie, Telico, Mamou 063, Guinea
[4] LIED Laboratory, UMR 8236 CNRS, Université Paris Cité, 35 rue Hélène Brion, 75006 Paris, France

e-mail: mohamed-lamine.toure@etu.univ-lehavre.fr; mamadou-bailo.camara@univ-lehavre.fr; maoulidafahad@gmail.com; alireza.payman@univ-lehavre.fr; brayima.dakyo@univ-lehavre.fr

Abstract — **Using photovoltaic (PV) energy in stand-alone micro-grid systems represents an effective solution for improving access to electricity in remote rural areas while reducing dependence on conventional power grids. This paper presents an energy management and control strategy for a PV–batteries micro-grid supplying an AC load through a three-phase voltage source inverter. The proposed system aims to maximize the solar energy production while ensuring reliable and stable operation of the micro-grid. The PV generator is modeled using a voltage model that considers the variation of the series resistance as a function of solar irradiance and operating temperature. To ensure optimal power extraction, a Maximum Power Point Tracking (MPPT) algorithm based on the incremental conductance method is implemented. A rule-based energy management system coordinates the power exchange between the PV generators and the batteries energy storage system. In addition, the DC-bus voltage is regulated using a proportional–integral controller through the bidirectional converter in batteries side, ensuring system stability under varying operating conditions. The DC power is converted into AC power by a two-level three-phase voltage source controlled using the space vector pulse width modulation (SVPWM) technique to provide high-quality output voltage with reduced harmonic distortion. The performances of the proposed system are evaluated through simulations using Matlab/Simulink software under different solar irradiance levels and load conditions. Simulation results demonstrate the effectiveness of the proposed control strategy in stabilizing the DC-bus voltage, maximizing PV power extraction, and mitigating power fluctuations through the batteries energy storage, thereby ensuring reliable power supply for rural micro-grid applications.**

Keywords — Photovoltaic system; battery energy storage; energy management system; DC-bus voltage regulation; space vector PWM (SVPWM); voltage source inverter; stand-alone micro-grid.

I. INTRODUCTION

Climate change worldwide, combined with the gradual depletion of fossil fuel resources, necessitates the implementation of sustainable energy solutions aimed at reducing our dependence on these polluting energy sources. In this context, the integration of renewable energies into stand-alone micro-grids emerges as an effective alternative for limiting greenhouse gas emissions while enhancing energy autonomy and reliability.

Among these sources, solar photovoltaic (PV) energy stands out particularly in the sub-Saharan region of West Africa. This case of study is focused to Republic of Guinea, which benefits from an average daily sunshine duration of 8 to 9 hours, representing a significant advantage for rural communities and areas located far from major national grid interconnections. Therefore, the development of solar integration solutions within these stand-alone micro-grids will facilitate access to electricity and promote the creation of income-generating activities.

However, the optimal operation of a photovoltaic generator remains complex due to its inherently variable and non-linear behavior, as well as the phenomena related to the penetration of solar radiation through the Earth's atmosphere. Indeed, the power output is highly dependent on environmental conditions, particularly solar irradiance and temperature. This makes the use of Maximum Power Point Tracking (MPPT) techniques essential to ensure optimal energy efficiency.

Several MPPT approaches have been developed, including the Perturb and Observe (P&O) method, the Incremental Conductance (InC) technique, and adaptive step-size methods, as presented in [1], [2], [3], [4]. Among these, the InC algorithm stands out for its ability to more effectively track the maximum power point, especially under conditions of high solar irradiance variability.

Furthermore, energy management of photovoltaic systems coupled with batteries Energy Storage Systems (ESS) requires the implementation of an Energy Management Strategy (EMS) capable of responding rapidly to efficiently direct energy either to the micro-grid or to the batteries. Various studies-based EMS approaches have proposed based on fuzzy logic, decision rules, or hierarchical architectures [4-13].

For instance, Swetha et al. [5] developed a centralized model-based strategy adapted to electric vehicle applications in a micro-grid environment. Similarly, Oukkacha et al. [6] proposed an energy management method based on frequency sharing among a fuel cell, lithium-ion batteries, and supercapacitors, all interfaced through DC-DC converters. Badawy and Sozer [7], on the other hand, designed and implemented an Energy Management Strategy Control (EMSC) for a micro-grid integrating renewable energy sources and batteries.

Moreover, Baqar et al. [8] conducted a comparative analysis of various EMSC strategies applied to a hybrid system combining a fuel cell, supercapacitors, and batteries, highlighting the importance of effective coordination to extend battery lifespan. Finally, Bonkile and Ramadesigan [9] proposed an autonomous energy management approach for a PV-battery hybrid system aimed at minimizing overload constraints using the Runge-Kutta method with high-stability time steps.

In terms of DC-bus voltage regulation, which is a key element in stand-alone micro-grid architectures, whether embedded or stationary, conventional controllers such as PI and PID remain widely used to ensure system voltage stability [10], [11]. In this context, Yaqoob et al. [12] proposed an energy management strategy based on plateau control for a stand-alone photovoltaic-battery hybrid system, with the objective of stabilizing the DC-bus voltage while optimizing power distribution among the different sources.

Similarly, an Energy Management Strategy and Control (EMSC) designed for a DC micro-grid integrating a photovoltaic module, batteries, and a load was developed in [13], aiming to optimize energy flows while extending battery lifespan. Furthermore, Benzaouia et al. [14] conducted an experimental evaluation of a control strategy for a PV/battery system dedicated to water pumping applications, using neural networks to maximize power extraction on the PV side and fuzzy logic on the battery side to maintain a balance between energy supply and demand.

Despite these advances, only a limited number of studies have combined an Incremental Conductance (InC)-based MPPT strategy with a PI controller dedicated to DC-bus voltage regulation within a PV/batteries/inverter architecture intended for stand-alone AC micro-grids. Furthermore, few works consider a photovoltaic system voltage model that incorporates a variable series resistance while also accounting for realistic weather conditions.

In this context, the present work proposes a hybrid PV/batteries/inverter system designed for stand-alone micro-grid applications. The developed energy management strategy is based on Incremental Conductance (InC) MPPT algorithm, enabling optimal extraction of photovoltaic power under variable irradiance conditions while accounting for the effect of the PV generator's series resistance.

This system is coupled with two PI controllers: the first ensures the DC-bus voltage regulation by effectively controlling the batteries charging and discharging through a bidirectional DC-DC converter, while the second, associated with a unidirectional DC-DC Boost converter, guarantees power transfer from the photovoltaic system to the DC-bus.

A two-level three-phase inverter is connected to the DC- bus and controlled using the SVPWM algorithm to ensure a reliable AC power supply for domestic loads.

The system is modeled and simulated in Matlab/Simulink using realistic climatic data, particularly solar irradiance and temperature measured at the Dialakoro pilot site in Republic of Guinea. The study aims to evaluate the performances of the micro-grid under various production and consumption scenarios, with a particular focus on the DC-bus voltage stability, the batteries safety, and the inverter operation to ensure an appropriate voltage supply with a frequency of 50 Hz.

The obtained results highlight effective regulation, efficient utilization of solar energy, optimal batteries energy management, and high-quality power delivered to consumers, thereby confirming the relevance of this approach for stand-alone micro-grid applications.

The paper is organized as follows: Section II presents micro-grid architecture, emphasizing the modeling of photovoltaic sources, batteries storage systems, and DC/AC conversion through a three-phase inverter. Section III is dedicated to energy management strategies which introduce the principle of MPPT control and adopted energy management strategy. Section IV presents simulation results and provides an in-depth analysis. Section V concludes the study by summarizing the main findings.

II. Description of Micro-grid

Figure 1 presents the overall architecture of the studied hybrid system, which includes a photovoltaic (PV) source characterized by a variable series resistance, a module of the batteries, a three-phase inverter, and a load represented by a household. The photovoltaic generator is connected to a boost converter, controlled by the Maximum Power Point Tracking (MPPT) strategy. This strategy relies on an algorithm that optimizes in real time the power extracted from the PV array by continuously adjusting the operating point.

The energy storage system consists of batteries connected to DC-bus through a bidirectional DC-DC converter, controlled by a dual PWM signal generated by the energy management system. This device enables batteries charging when photovoltaic production exceeds demand and discharging to supply the load when solar generation is insufficient.

Furthermore, a three-phase inverter, controlled using the SVPWM technique, ensures the conversion of energy from the DC-bus to the AC bus. It consists of three legs, each comprising two IGBT switches that are driven in a complementary manner to generate an alternating voltage or current at the desired frequency, set to 50 Hz in this case.

The considered micro-grid as the main load, is supplied through the AC bus, whose voltage is regulated via coordinated power management across all converters. This architecture enables both intelligent and adaptive energy management, facilitating the integration of the photovoltaic system into a stand-alone micro-grid, while enhancing energy flexibility.

A. Behavior Modeling of Solar PV

$$\begin{cases} V_{pv} = \alpha \cdot \dfrac{n \cdot k \cdot T}{q} \cdot \ln\left(\dfrac{I_{ph} - \frac{I_{pv}}{N_{p,ch}} \cdot k_{\lim i}}{N_{sc} \cdot I_o} \cdot \beta + 1 \right) - I_{pv} \cdot R_s \cdot \lambda \\ \alpha = N_{s,ch} \cdot N_{sc} \\ \beta = \left(\dfrac{T}{T_{ref}} \right)^3 \cdot \exp\left(\dfrac{q \cdot E_g \left(\frac{1}{T_{ref}} - \frac{1}{T} \right)}{n \cdot k} \right) \\ \lambda = \dfrac{N_{s,ch} \cdot N_{sc} \cdot k_{\lim v}}{N_{p,ch}} \\ k_{\lim i} = \dfrac{I_{sc} - I_{mp}}{I_{mp}} \\ k_{\lim v} = \dfrac{V_{oc} - V_{mp}}{V_{mp}} \end{cases} \quad (1)$$

Several mathematical models of PV panels have been developed with the aim of accurately representing their electrical properties and operation, which derive directly from the physical structure of PV cells as in [15], [16]. In this study, the used PV model is based on the methods described in [3],[1]. The PV voltage model with variable series resistance is connected directly to the DC-bus via a boost converter, thus guaranteeing power transfer from the PV string to the DC-bus. Table I presents the main technical characteristics of the PV module and DC-DC boost converter. In addition, the voltage-current (I-V) properties of the PV panel, and the links with power output, can be explained using equation (1), which summarizes the electrostatic behavior of the module under standard irradiance and temperature conditions, where I_{pv}, V_{pv}, I_o and I_{ph} present respectively the PV current, voltage, saturation current and photocurrent. The series and parallel resistances are R_p and R_s. N_s and N_p are the total number of solar modules connected in series and parallel respectively. T is the PV surface temperature. n, E_g and k are the ideality factors, gap energy and Boltzmann constant, respectively.

TABLE I. CHARACTERISTICS OF PV PANEL AND BOOST CONVERTER

Electrical Parameters	Values
Solar PV source	
Maximum power P_{mpp}	*345 W*
Maximum Current I_{mpp}	*9.05 A*
Short-circuit current I_{sc}	*9.52 A*
Maximum voltage V_{mpp}	*38.14 V*
Open-circuit Voltage Voc	*46.52 V*
Temperature coefficient of current k_{sc}	+0.049 % /°C
Temperature coefficient of voltage k_{oc}	-0.315 % /°C
Series cells *Nsc*	72
Number of modules in series in a PV string $Ns_{,ch}$	7
Number of parallel strings in a PV string $N_{p,ch}$	80

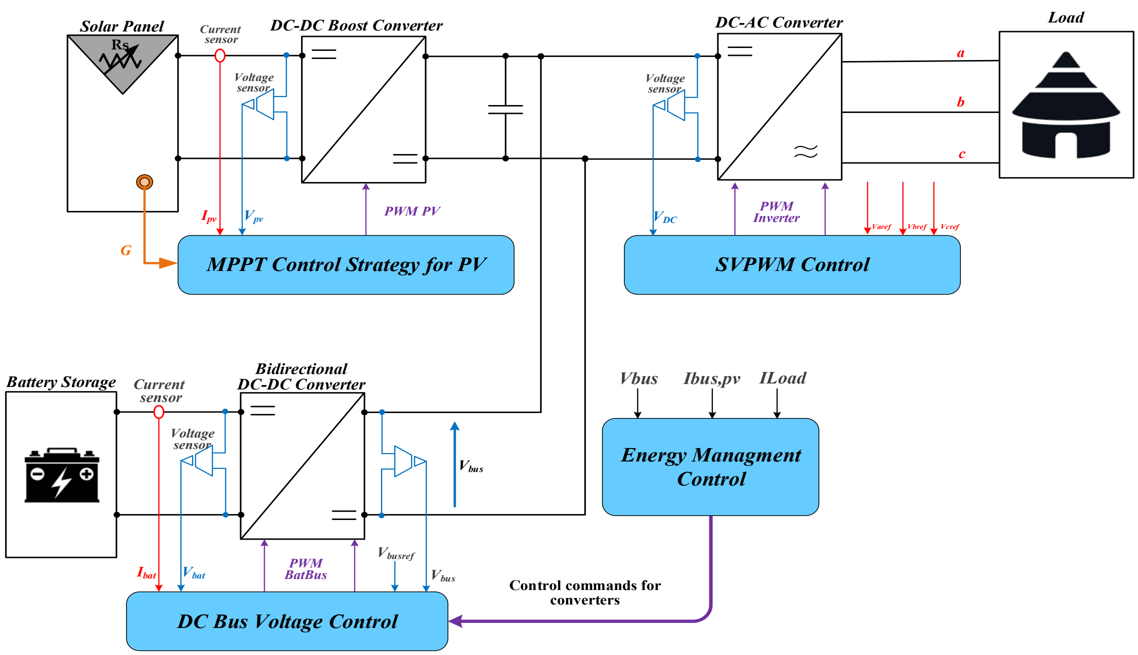

Fig. 1. Proposed power system topoloy.

B. Behavior Modeling of the Batteries

The batteries are high energy density, quick dynamic response, and low rate of self-discharge make it a promising technology for storing renewable energy in hybrid systems. As depicted in Fig. 1, the batteries are connected to the DC-bus via a bidirectional DC-DC converter, enabling efficient DC power supply to the load. The considered model of the batteries is presented in equation (2), [17], [18].

$$\begin{cases} V_{bat} = E_0 - K \cdot \dfrac{Q}{Q-it}\, it - R_b \cdot i_{bat} + A_b\, e^{-B\cdot it} - K \cdot \dfrac{Q}{Q-it}\, i^*(\text{Discharge}) \\ V_{bat} = E_0 - K \cdot \dfrac{Q}{Q-it}\, it - R_b \cdot i_{bat} + A_b\, e^{-B\cdot it} - K \cdot \dfrac{Q}{it+0.1Q}\, i^*(\text{Charge}) \end{cases} \tag{2}$$

With $it = \int_0^t i_{bat} dt$ and $i^* = LFP(i_{bat})$

In equation (2), the open-circuit voltage is denoted by E_0. Q is the capacity (Ah) of a typical battery. i_t is the battery's current charge (Ah). The polarization constant is denoted by K. The exponential zone amplitude (in V) is shown by A_b. B represents the exponential zonetime constant inverse in the exponential zone (Ah)$^{-1}$. The internal resistance (in Ω) is denoted by R_b. The battery's current is denoted by i_{bat}, and the filtered current (in A) by i^*.

The battery design was modeled using simulation based on the technical specifications listed in Table II, which also includes the parameters of the bidirectional DC-DC converter. The model describing the battery's state of charge SoC_{bat}, is evaluated using equation (3) [18], [19], where SoC_{bat} is the battery state of charge (%), Q_{bat} is the maximum battery capacity (Ah).

$$SOC_{bat} = 100 \cdot \left(1 + \frac{1}{Q_{bat}} \cdot \int_0^t i_{bat}(t)\, dt \right) \tag{3}$$

The battery's charge-discharge cycle is mainly determined by the amount of power available and the power level required by the system. This cycle depends on both available energy capacity and demand dynamics. The battery's State of Charge (*SoC*) limits are used to define operational constraints, framing minimum and maximum operating thresholds. These limits are used to set safety limits and optimize battery use according to the actual power capacities that can be supplied or absorbed at any given time, as described in equation (4), where SoC_{batmin} and SoC_{batmax} are respectively the state of charge minimum and maximum.

$$SOC_{bat\,\min} \leq SOC_{bat} \leq SOC_{bat\,\max} \quad (4)$$

TABLE II. CHARACTERISTICS OF BATTERY AND BIDIRECTIONAL CONVERTER

Electrical Parameters	Values
Battery source	
Battery capacity: Q	648 Ah
Constant voltage: E_0	273.2 V
Polarization constant: K	0.0029 (V/Ah)
Battery internal resistance R_b	0.0038 (Ω)
Exponential zone amplitude A_b	21.16 (V)
Exponential zone time constant inverse B	0.094 $(Ah)^{-1}$
SOCbat	50%

C. Modeling of the DC–AC Converter

The considered DC-AC converter is based on two-level three-phase inverter designed to convert the energy from the DC-bus into alternating current (AC) suitable for supplying domestic loads. It consists of three legs corresponding to the three phases, each including two power switches based on IGBT technology equipped with antiparallel diodes. Inverter is controlled using the Space Vector Pulse Width Modulation (SVPWM) technique, which enables the generation of a quasi-sinusoidal three-phase voltage, thereby improving power quality while reducing harmonic distortion.

Furthermore, an LC filter is installed at the inverter output to smooth the voltage and current waveforms by attenuating the harmonic components generated by the switching of the power devices. This filtering significantly improves the quality of the supplied energy by ensuring a voltage waveform closer to a pure sinusoid at a frequency of 50 Hz, making it suitable for stand-alone micro-grid applications (Fig. 2).

III. Energy Management Strategies

This section provides an in-depth explanation of the MPPT control principle, and the energy management strategy proposed in this paper.

A. Principle of MPPT Control for PV

The photovoltaic (PV) panel, as a generator of electrical energy, converts solar irradiance into electricity through a direct conversion process. Nevertheless, this conversion is subject to the intrinsic variability of solar resources, which induces intermittent and non-linear behavior in energy production. This characteristic adversely affects the stability and performance of the PV system. To mitigate these effects and optimize energy capture, the integration of a dedicated control system is essential.

To do this operation, the MPPT algorithms play a crucial role, adapting the operating point of the PV system in real time to extract the maximum available power. Several MPPT strategies have been proposed in the literature [3], [20], [21], aiming to autonomously control the voltage of each PV module, in order to maximize energy efficiency under varying sunlight and temperature conditions.

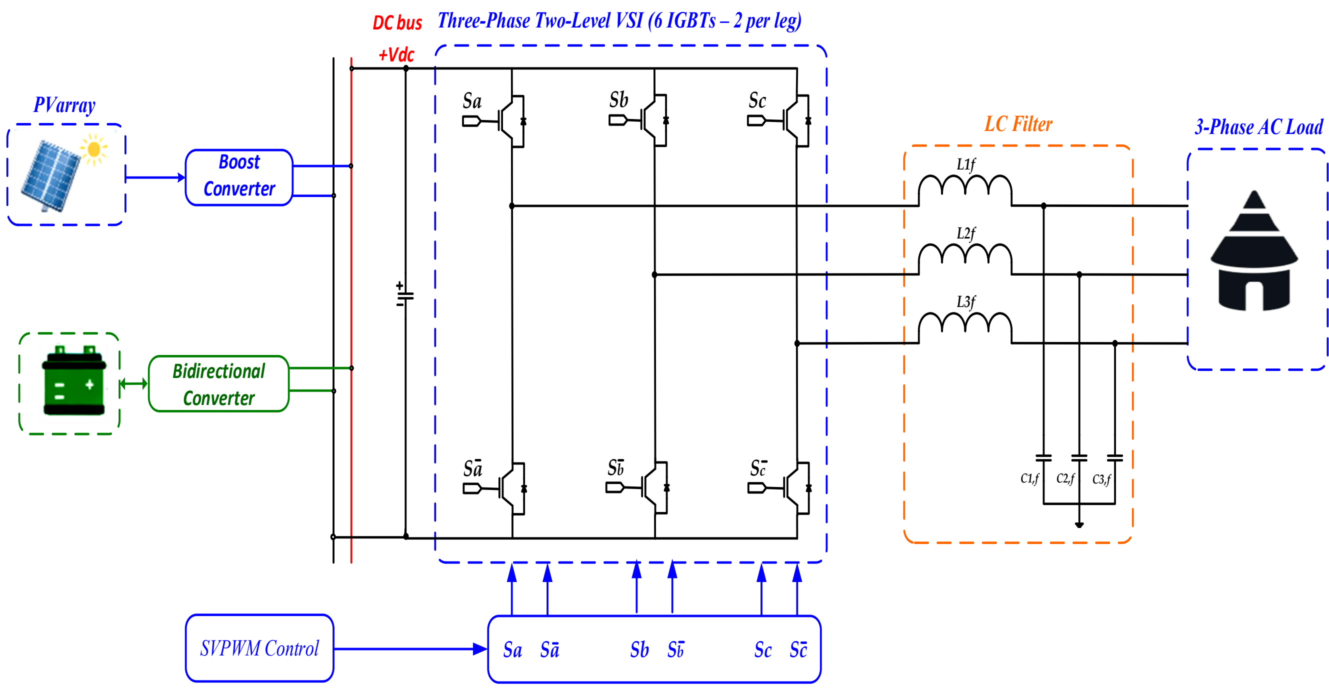

Fig. 2. DC–AC inverter structure and control.

In the present work, the authors have opted for the control strategy with the integrated Incremental Conductance (InC) algorithm, whose principle is illustrated in Fig. 3, as the method for tracking the maximum power point. The InC algorithm is based on an analysis of the power gradient as a function of voltage (*dP/dV*), enabling precise estimation of the optimum operating point. In combination with the irradiance sensor, it provides the reference current that is calculated using equation (5). Figure 4 presents the Incremental Conductance (InC) MPPT algorithm.

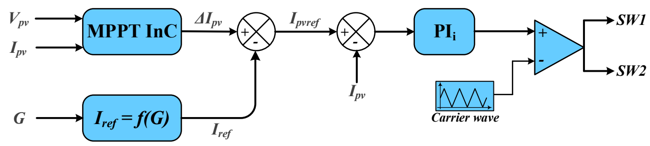

Fig. 3. MPPT Control Strategy.

$$I_{ref} = \left(I_{sc} + k_{sc} \cdot (T - 298.15)\right) \cdot \left(\frac{G}{1000}\right) \tag{5}$$

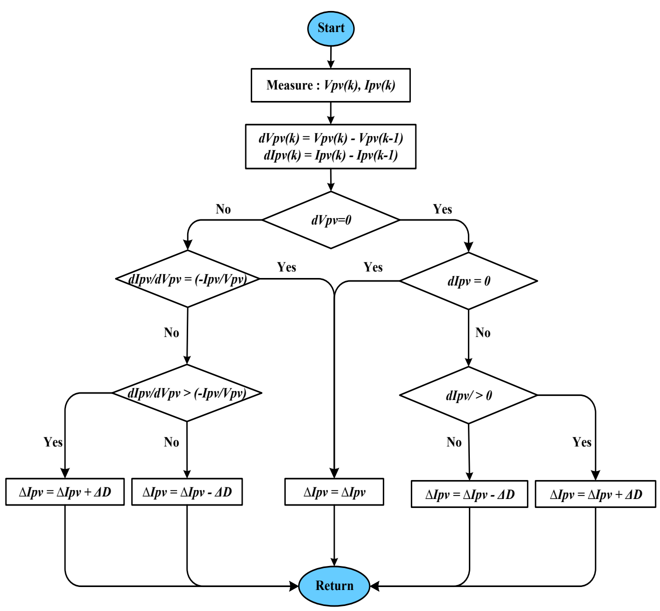

Fig. 4. Diagram of the InC MPPT.

B. Energy Management Strategy and Control (EMSC)

The objective of this study is to develop an energy management strategy within a micro-grid based on the use of a Proportional-Integral (PI) controller, to optimize energy exchanges between the different components of the system. A key aspect of this approach is to ensure the stability of the DC-bus voltage, which must be maintained at a predefined reference level despite external disturbances and inherent system uncertainties. Indeed, controlling this voltage is essential to guarantee the proper operation, reliability, and safety of the micro-grid.

The proposed method is based on minimizing the deviation between the measured DC-bus voltage V_{bus} and its reference value V_{busref} through a robust and structured control strategy. The operation of the micro-grid requires continuous adaptation to fluctuations in photovoltaic power generation. In this context, the batteries energy management plays a crucial role in preventing system instabilities caused by excess or insufficient production, while ensuring a continuous balance between energy supply and demand.

Since the batteries module is connected to the DC-bus through a bidirectional DC-DC converter, the main role of the PI controller is to operate this converter in either buck or boost mode, depending on the energy requirements. The reference current, generated by the PI voltage controller, is then used to determine the duty cycle applied to the pulse-width modulation (PWM) module, thereby ensuring effective control of the converter.

As illustrated in Fig. 2, photovoltaic energy is first injected into the DC-bus of the micro-grid and then delivered to the load through an inverter. In the event of excess production, the surplus energy is stored in the batteries. The power transfer from the DC-bus to the load is ensured by the inverter, whose control, combined with an LC filter at its output, improves the quality of the energy supplied to the consumer.

This strategy ensures accurate regulation of both current and voltage while maintaining an overall energy balance. It promotes optimal using of solar energy due to batteries assistance.

The structure of the control illustrated in Fig. 5, is based on a PI control loop that generates the appropriate duty cycle to ensure tracking of the reference voltage V_{busref}, set at 1000V. This approach enables the batteries charging and discharging processes without the degree of freedom limit due to cascade control architectures.

The k_p and k_i parameters of the proportional-integral controllers applied to the photovoltaic current and the DC-bus voltage were determined using equation (6) to optimize the dynamic response of the system. The optimal values obtained for these coefficients are presented in Table III. The system performance is subsequently tested through simulations.

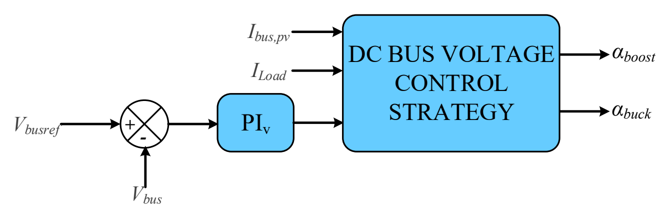

Fig. 5. DC-bus voltage control.

$$\begin{cases} k_{pi} = L \cdot \omega_n^2 \\ k_{ii} = 2 \cdot \varepsilon . L \cdot \omega_n^2 \\ k_{pv} = C \cdot \omega_n^2 \\ k_{iv} = 2 \cdot \varepsilon . C \cdot \omega_n^2 \end{cases} \quad \begin{cases} \omega_n = 2 \cdot \pi \cdot \frac{f}{10} \\ \varepsilon = \frac{\sqrt{2}}{2} \\ \tau_{(i,v)} = \frac{k_{p(i,v)}}{k_{i(i,v)}} \end{cases} \tag{6}$$

The current and voltage control bandwidth ω_n is fixed to 10% of that the converters control frequency [5], [7].

Figure 6 presents the flowchart of the proposed control strategy. The batteries energy storage system performs a dual function, both supplying energy when required and absorbing excess production. In stand-alone mode, when generation exceeds demand, the algorithm controls the batteries charging process while respecting its safety constraints, particularly the maximum allowable current.

TABLE III. PI CONTROLLER PARAMETERS

Coefficients	Values
k_{pi}	0.1
k_{ii}	100
k_{pv}	0.1
k_{iv}	1
f	10kHz
L	1mH
C	3300µF

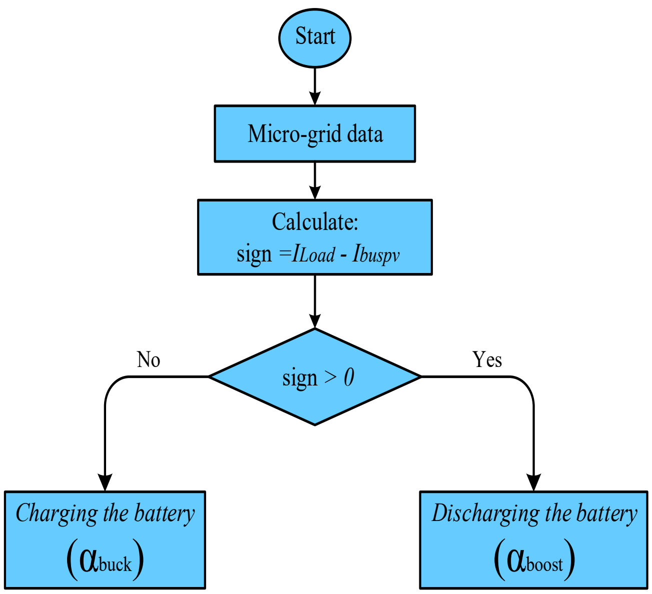

Fig. 6. Voltage control strategy.

Conversely, in the event of insufficient photovoltaic generation, the batteries supply the required energy to meet the load's demand until its discharge limit is reached. Furthermore, the energy management system continuously monitors the batteries state of charge, thereby ensuring reliable and secure operation of the micro-grid.

C. Control of Inverter Using SVPWM

Grid-connected PV systems represent a key solution for sustainable energy production; however, their efficient integration requires advanced power conversion and control strategies. In [22], a new three-phase three-level NPC (Neutral Point Clamped) inverter structure combined with the SVPWM (Space Vector Pulse Width Modulation) technique is proposed for injecting PV energy into the grid without storage, using a high-gain interleaved Boost converter. The results demonstrate a high efficiency of 96.1%, although the output voltage THD (Total Harmonic Distortion) remains relatively high (22.33%).

In [23], an MPPT control strategy based on the incremental conductance algorithm combined with a dual closed-loop technique is developed for a hybrid PV-battery microgrid, improving power tracking, energy flow management, and DC-bus voltage regulation in accordance with the EN50530 standard. Similarly, [24] proposes an improved MPPT approach coupled with *d-q* current regulation to stabilize the DC-link voltage and reduce harmonics; however, the absence of THD results limits a comprehensive evaluation of its performance.

Furthermore, [25] introduces an advanced Fractional Order Integral Sliding Mode Control (FOISMC) strategy optimized using the Particle Swarm Optimization (PSO) algorithm, applied to a PV system including a DC-DC converter and a three-phase inverter. This approach significantly enhances system dynamic performance, achieving notable reductions in voltage, active and reactive power, as well as overshoot and response time, highlighting the effectiveness of intelligent control techniques.

Finally, [26] emphasizes the importance of multilevel inverters in large-scale PV plants, showing that the choice of topology (CHB – Cascaded H-Bridge, NPC – Neutral Point Clamped, FC – Flying Capacitor) has a significant impact on overall system performance. While the CHB topology offers better voltage tolerance, NPC and FC structures simplify the system by eliminating the need for multiple DC sources. Overall, these studies demonstrate that improving PV system performance relies on a synergy between inverter topologies, control strategies, and modulation techniques, paving the way for more efficient, stable, and grid-compliant energy systems.

In this study, the authors propose SVPWM control as an inverter management strategy for the grid. SVPWM algorithm presented in Fig. 7 first converts the three-phase reference voltages into the stationary $\alpha\beta$ reference frame using the Clarke transforming.

The reference voltage vector is then located within one of the six sectors of the space vector diagram. The dwell times of the adjacent active vectors and zero vectors are calculated to synthesize the reference voltage during each switching period. Finally, the corresponding duty cycles are used to generate the gating signals for the six IGBT switches of the two-level inverter.

The sector identification is performed using a decision-based algorithm that avoids the computation of the arctangent function. The algorithm determines the sector of the reference voltage vector in the $\alpha\beta$ plane by analyzing the signs of V_α and V_β and comparing the ratio V_β/V_α with $\sqrt{3}$ as presented in Fig. 8. This method significantly reduces the computational complexity and is suitable for real-time implementation of the SVPWM strategy.

The proposed inverter is a two-level three-phase voltage source inverter connected to DC-bus and designed to deliver 150 kW/ 400 V AC/50 Hz three-phase AC load. A switching frequency of 10 kHz is adopted for the SVPWM signal generation. To improve the output voltage quality, an LC filter composed of a 1 mH phase inductance and a 25 µF phase capacitor is used. The DC-bus capacitor in inverter input is fixed to 2 mF to ensure DC-bus voltage stability.

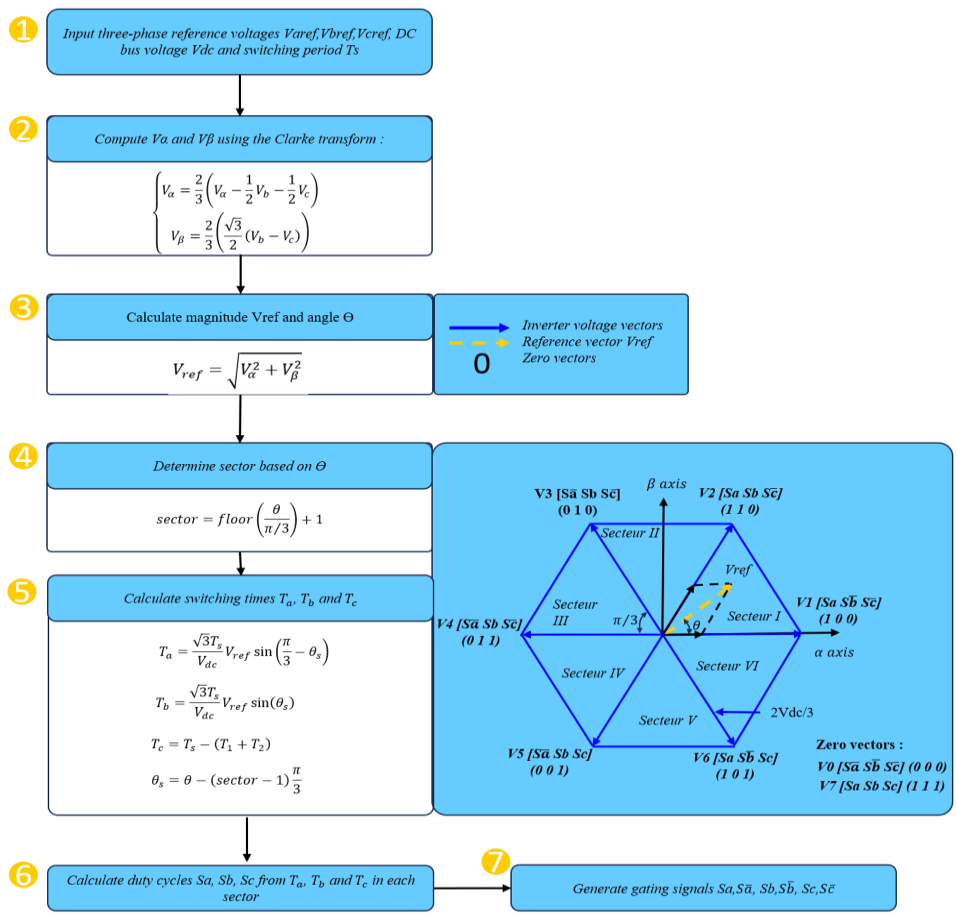

Fig. 7. Space Vector PWM Algorithm.

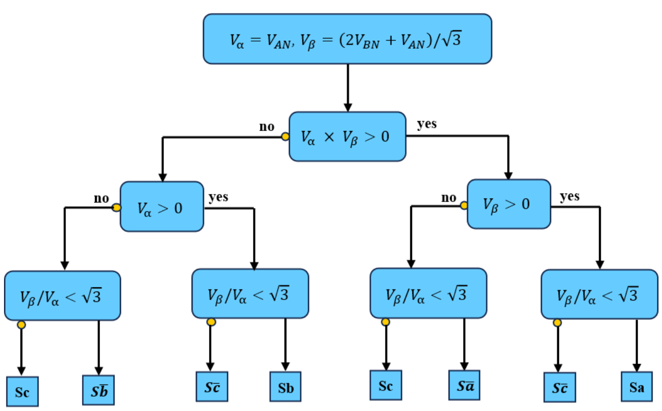

Fig. 8. Decision algorithm for sector identification in the SVPWM control strategy.

In order to accurately reproduce the dynamic behavior of the load, a time-varying current profile is imposed on the three-phase system. The studied system consists of a three-phase voltage source inverter supplied by a DC-bus voltage V_{dc} of $1000V$ .The inverter generates a three-phase AC voltage with a line-to-line RMS value is given in equation (7),

$$V_{LL} = \frac{m * V_{DC}}{\sqrt{3}} \quad (7)$$

at a fundamental frequency of 50 Hz.
For a balanced three-phase system, the phase voltage is given in equation (8),

$$V_{ph} = \frac{V_{LL}}{\sqrt{3}} \quad (8)$$

which yields $V_{ph} \approx 231$ V for $V_{LL} = 400V$ and $m = 0.69$.

TABLE IV. INVERTER PARAMETERS

Electrical Parameters	**Values**
Inverter	
Switching frequency fsw	*10 kHz*
Modulation index (SVPWM)	*0.69*
Output frequency	*50Hz*
Sampling time	*10^{-5} s*
SOCbat	*50%*
LC Filter at output of the inverter	
Filter inductance L_{1f}, L_{2f}, L_{3f}	*1 mH*
Filter capacitance C_{1f}, C_{2f}, C_{3f}	*25 μF*

The natural frequency of the filter is given in equation (9).

$$f_c = \frac{1}{2\pi\sqrt{L1f.C1f}} \quad (9)$$

Thus, for the selected filter values in our system, the cutoff frequency f_c, after calculation, is approximately 1006Hz.

IV. Simulation Results and Discussion

After modeling the PV system, the energy storage device, the inverter, and the various control strategies, Matlab/Simulink software was used to implement and simulate the hybrid energy system to evaluate the performances of the proposed energy management strategy.

The DC-bus side is characterized by the interaction between the photovoltaic system and the batteries through the main DC-bus, via the respective Boost and Buck-Boost converters, which enable continuous power flow management through their control algorithms. The simulated climatic conditions presented in Fig. 9 include the variations of solar irradiance (in W/m²), and ambient temperature (in °C) as well as load's demand over a period of 1000 hours. These parameters affect the energy production of photovoltaic modules.

The load current profile I_{Load}, shown in Fig. 10, is interpolated and applied at the inverter output in a stepwise manner. This implementation is carried out using the *Three-Phase Breaker* and *Three-Phase Series RLC Branch* blocks in MATLAB/Simulink, configured in resistive mode, in order to accurately reproduce the real dynamic behavior of the measured load.

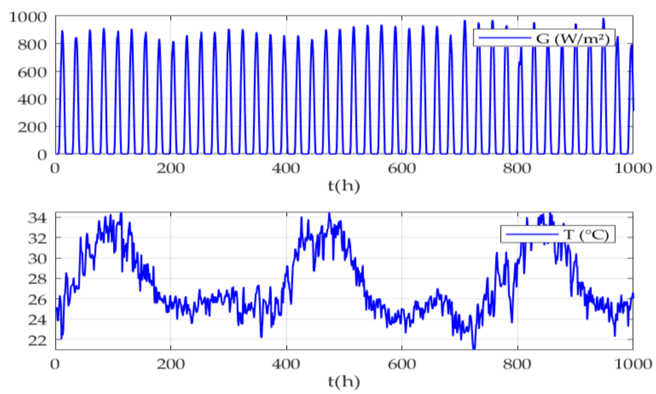

Fig. 9. Variations in experimental weather conditions, solar radiation, temperature.

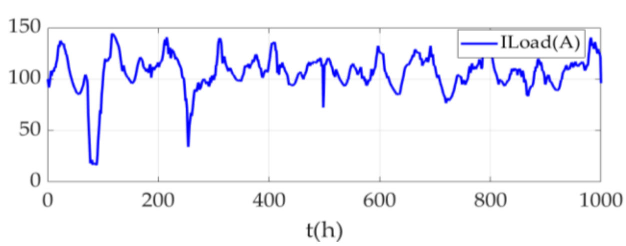

Fig. 10. Measured Load Current Profile

The curves presented in Fig. 11 show the temporal evolution of the PV modules voltage *Vpv* and its current I_{pv}. It can be observed that the system effectively responds to variations in irradiance and temperature, thereby ensuring optimal energy production. These results highlight the ability of the MPPT algorithm, along with the Boost converter control strategy, to dynamically adjust the operating point of the photovoltaic generator.

The waveforms illustrated in Fig. 12 highlight the measured current at the output of the PV array and the reference current generated by the MPPT controller through irradiance data provided by a pyranometer. The strong agreement between these two signals demonstrates the effectiveness of the incremental conductance algorithm, which is capable of rapidly adapting the reference current to variations in solar irradiance, thereby ensuring optimal energy production efficiency.

The DC-bus voltage is maintained around a reference value set at 1000 V. Its evolution during the simulations is presented in Fig. 13. Thanks to the action of the PI controller combined with the adopted control strategy, effective DC-bus regulation is achieved even in the presence of disturbances arising from the load connected to the inverter or from PV generation. Maintaining this voltage is essential to ensure the proper operation of all supplied devices, particularly the micro-grid loads.

The waveforms illustrated in Fig. 14 highlight the batteries behavior in response to system demands. The variations of the current correspond to the charging and discharging phases, depending on the availability of solar energy and the consumption requirements. The voltage remains within nominal ranges, reflecting the proper sizing of the bidirectional converter as well as the reliability of the energy management strategy.

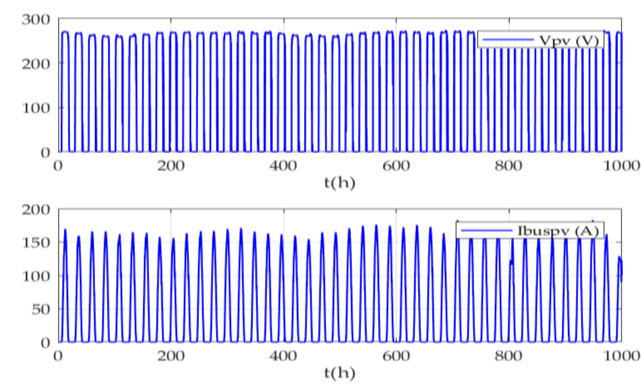

Fig. 11. Waveform of the current and voltage on the PV side.

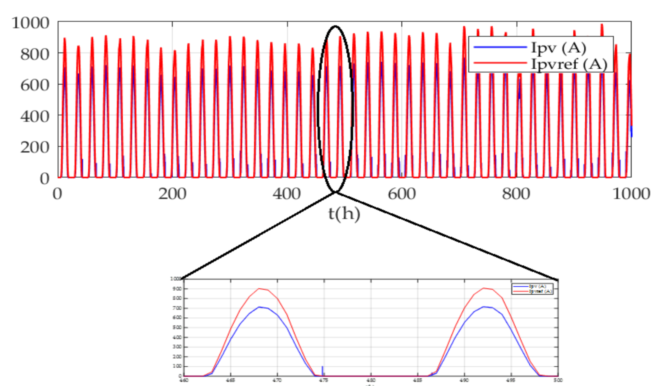

Fig. 12. Waveform of the current and its reference on the PV side.

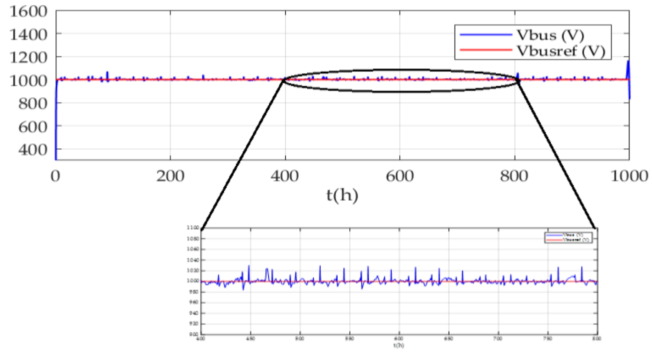

Fig. 13. DC-bus voltage.

The voltage across the batteries module terminals presented in Fig. 15 fluctuates around 269V, which is very close to its nominal value of 270 V. This slight decrease in voltage is due to the voltage drop caused by its internal resistance. The power supplied by the PV and batteries system is illustrated in Fig. 16. This result is obtained by emulating the real load profile on the DC-bus. The power compensation provided by the batteries when the PV power is zerocorresponds in practice to the period between sunset and sunrise.

Figure 17 shows the evolution of the three-phase currents i_a, i_b, i_c and the three-phase phase-to-neutral voltages at the inverter output v_a, v_b, v_c are presented in Fig. 18. Over the entire study period, amplitude variations are observed in both currents and voltages, reflecting the system's adaptation to fluctuations of the PV power and load demand. The zoom over the interval $t = 464.4\,s$ to $t = 464.44\,s$ highlights perfectly sinusoidal waveforms, balanced and phase-shifted by 120° between the three phases, which is characteristic of proper three-phase operation. It is important to emphasize that this current amplitude enables the simultaneous supply of multiple domestic loads or households in rural areas.

The similarity between the voltage waveforms v_a, v_b, v_c and the current waveforms i_a, i_b, i_c is explained by the resistive nature of the load, for which the current is proportional to the voltage. Furthermore, the regularity of the signals and the absence of significant distortion confirm the effectiveness of the SVPWM control strategy as well as the LC filter at the inverter output. These results demonstrate the high quality of the energy delivered to the micro-grid, in agreement with the low total harmonic distortion values.

Figure 19 presents the evolution of the duty cycles T_a, T_b, and T_c, normalized with respect to the switching period T_s, as well as the switching sector generated by the SVPWM control strategy applied to the three-phase inverter. Over the entire simulation period, the duty cycles vary continuously according to the system operating conditions, particularly fluctuations in photovoltaic generation and load's demand, while the sector variable takes inter values between 1 and 6 as illustrated in Fig. 20, corresponding to the different regions of the $\alpha\beta$ vector plane. The zoom over the interval $t = 464.4\, s$to $t = 464.44\, s$hlighlights periodic waveforms of the duty cycles, bounded between 0 and 1 and phase-shifted among the three phases, reflecting the time distribution of active and zero voltage vectors.

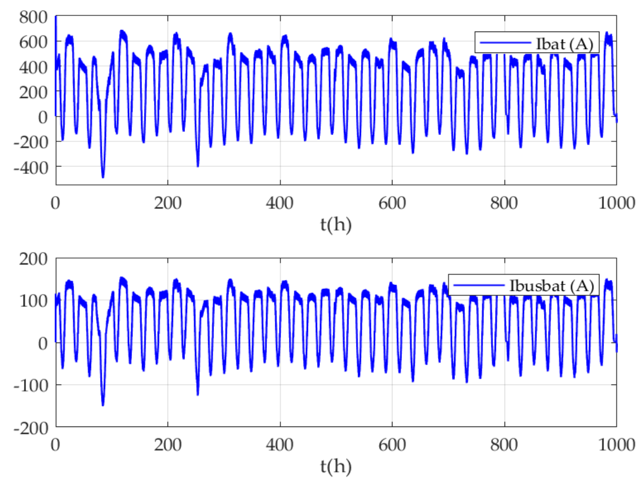

Fig. 14. Battery current input and output Waveform

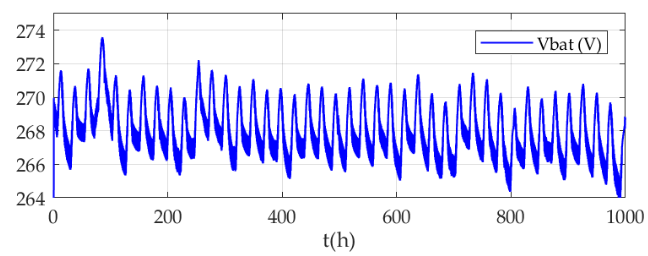

Fig. 15. Waveform of the voltage and current on the battery side.

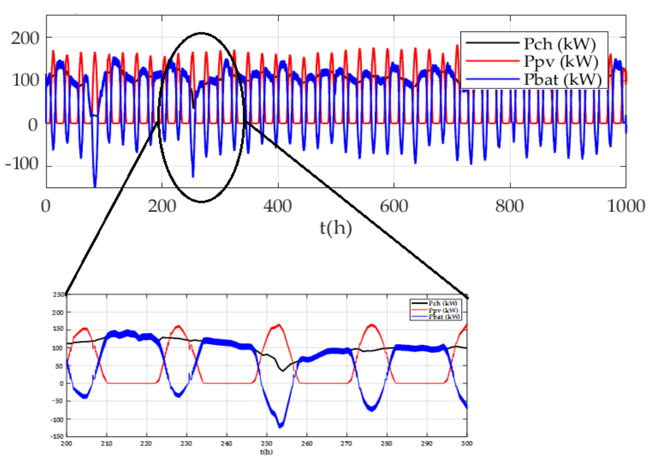

Fig. 16. Waveform of the power.

At the same time, the ordered succession of sectors reflects the continuous rotation of the reference voltage vector in the complex plane. Each sector transition corresponds to a new combination of active vectors, ensuring an accurate synthesis of the desired three-phase voltage. This coordination between duty cycles and sector selection confirms the correct operation of the SVPWM algorithm. It ensures optimal utilization of the DC-bus voltage, efficient switching of the power devices, and a significant reduction of harmonic content. Consequently, these results demonstrate the capability of the control strategy to generate balanced, high-quality three-phase voltages, contributing to the overall performance improvement of the system.

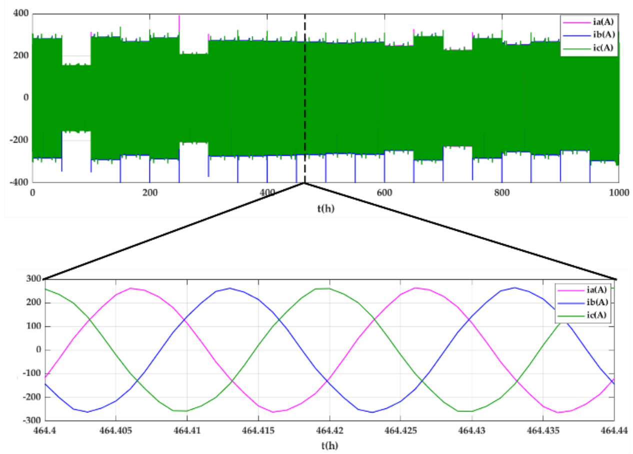

Fig. 17. Inverter output current.

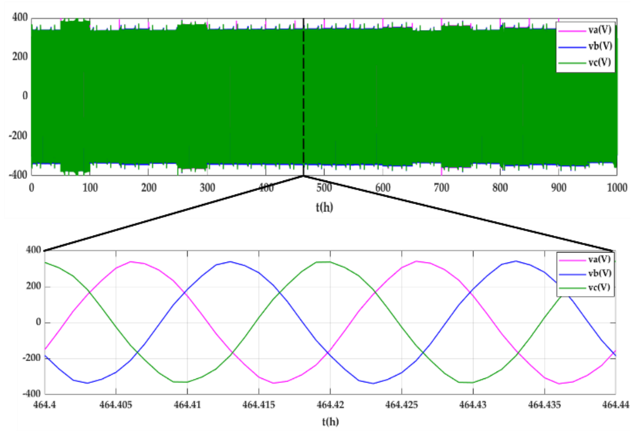

Fig. 18. Inverter output voltage.

Figures 21-23 present the PWM control signals of the inverter switches (S_1, S_4, S_3, S_6, S_5, S_2) along with the associated reference voltages ($V_{a,ref}, V_{b,ref}, V_{c,ref}$). Over the entire simulations period, the PWM signals appear as high-frequency rectangular waveforms, reflecting the rapid switching of the power devices, while the reference voltages maintain a sinusoidal shape. The zoom over the interval $t = 464.4\ s$ to $t = 464.44\ s$ highlights the fundamental principle of SVPWM modulation: the comparison between an implicit triangular carrier waveform and the sinusoidal reference signals, resulting in time-varying duty cycles. It can be observed that the pulse widths continuously vary according to the instantaneous amplitude of the reference voltages, enabling the reconstruction, after filtering, of balanced sinusoidal three-phase voltages.

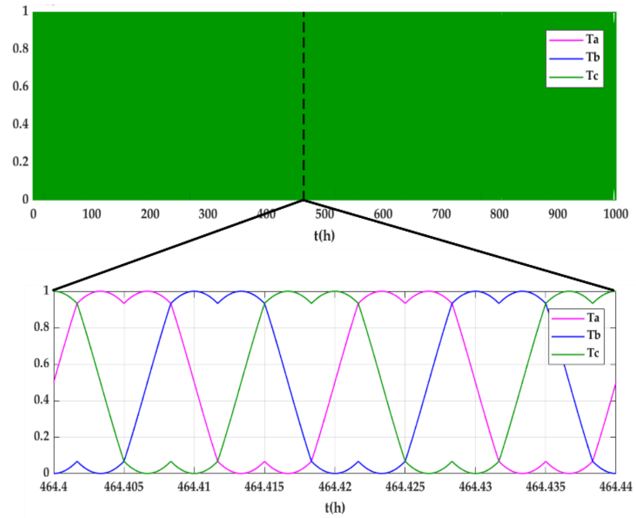

Fig. 19. Space vector PWM principle and switching sequence.

The complementary switching signals (S_1/S_4, S_3/S_6, S_5/S_2) ensure alternate control of the switches in each inverter leg, guaranteeing the proper synthesis of voltage levels. This pulse-width modulation accurately reflects the trajectory of the reference voltage vector in the $\alpha\beta$ plane, in accordance with the SVPWM principle.

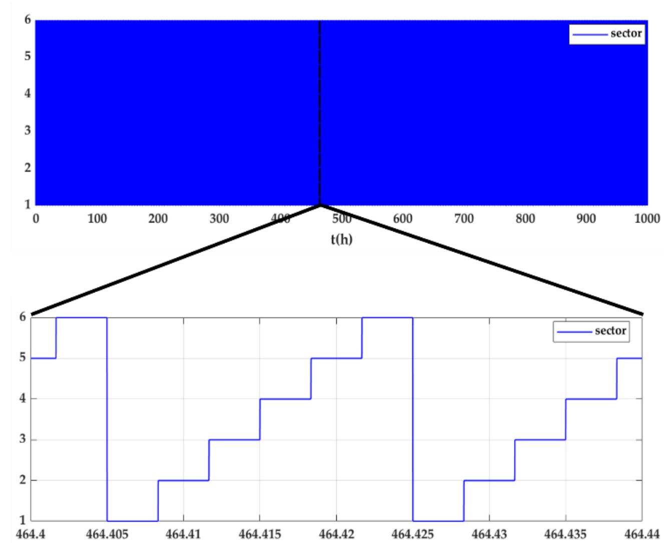

Fig. 20. Waveform sector

The consistency between the PWM signals and the reference voltages confirms the correct operation of the control algorithm. It ensures optimal utilization of the DC-bus voltage, efficient switching of the devices, and a significant reduction in harmonic contents. Consequently, these results demonstrate the capability of the SVPWM strategy to generate high-quality three-phase voltages, contributing to the overall performance improvement of the system.

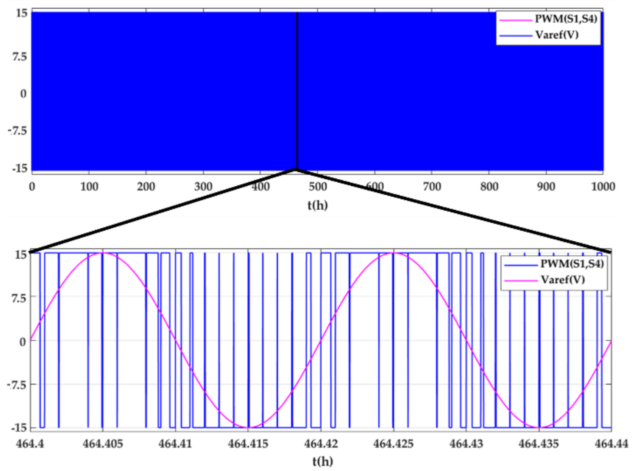

Fig. 21. PWM waveform and reference voltage Varef

Figure 24 shows the temporal evolution of the active power *P* supplied to the system over a period of 1000 hours on the DC-bus. It can be observed that the power varies dynamically according to operating conditions, particularly due to the power fluctuations of the PV and load in. The maximum power reached is approximately 150kW, which corresponds to the system's maximum capacity. The power variations reflect changes in operating conditions, particularly transitions between different levels of solar irradiance and load demand. The rapid oscillations observed around the power levels are associated with converter switching phenomena and control actions, without significantly affecting the overall stability of the system. Despite these fluctuations, the power remains generally well-regulated around consistent levels, highlighting the effectiveness of the energy management strategy. The system ensures an appropriate distribution of the power between the PV, the batteries storage, and the load, while respecting the maximum power limit and maintaining stable operation of the micro-grid.

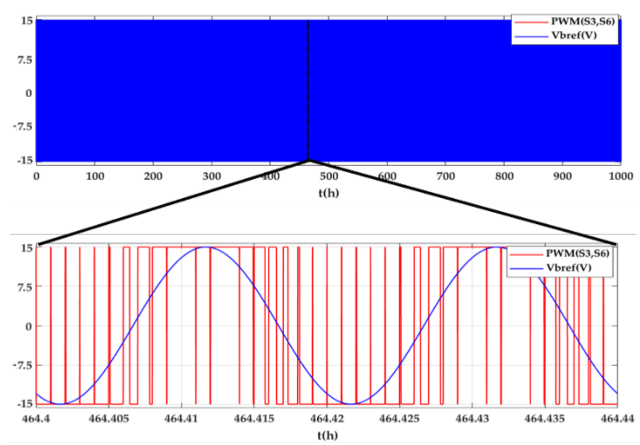

Fig. 22. PWM waveform and reference voltage Vbref

Figures 25 and 26 present the frequency analysis of the currents i_a, i_b, i_c as well as the voltages v_a, v_b, v_c at the inverter output, obtained using Fourier transform (FFT). It can be observed that the spectrum is dominated by the fundamental component at 50 Hz, corresponding to the grid frequency, while the harmonic components are very low. The total harmonic distortion (THD) values are around 2.4% for all phases, for both currents and voltages.

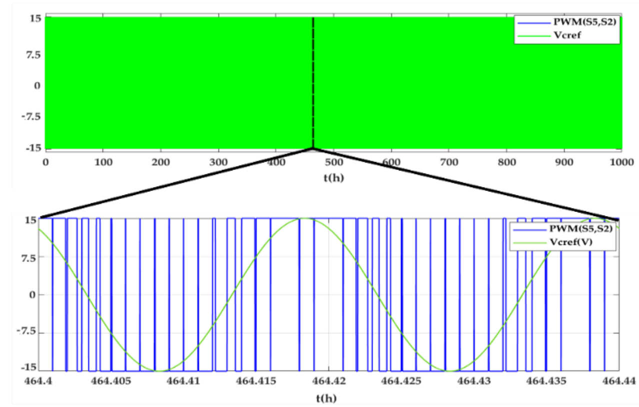

Fig. 23. PWM waveform and reference voltage Vcref

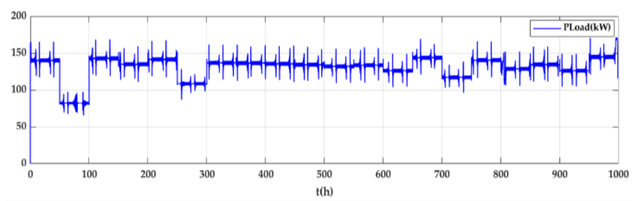

Fig. 24. Dynamic variation of load power.

The similarity of THD values between currents and voltages is explained by the resistive nature of the load, for which the current is proportional to the voltage, resulting in similar waveforms. Furthermore, the low amplitude of harmonics highlights the effectiveness of the SVPWM control strategy as well as the LC filter at the inverter output, which significantly attenuate the high-frequency components generated by switching. These results demonstrate a good power quality delivered to the micro-grid, meeting power quality standards, and confirm the adequacy of the filter design as well as the adopted control strategies.

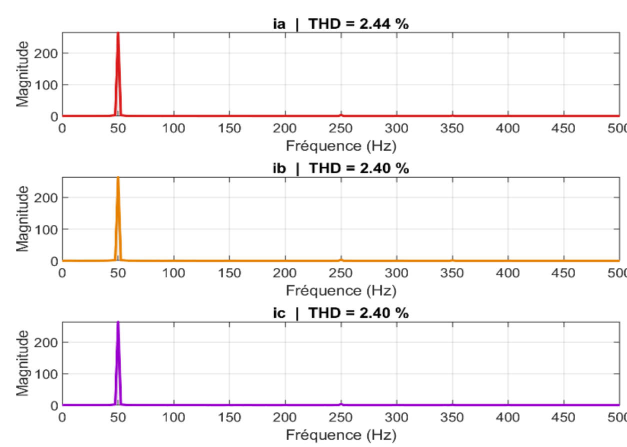

Fig. 25. Frequency analysis of the currents ia,ib and ic

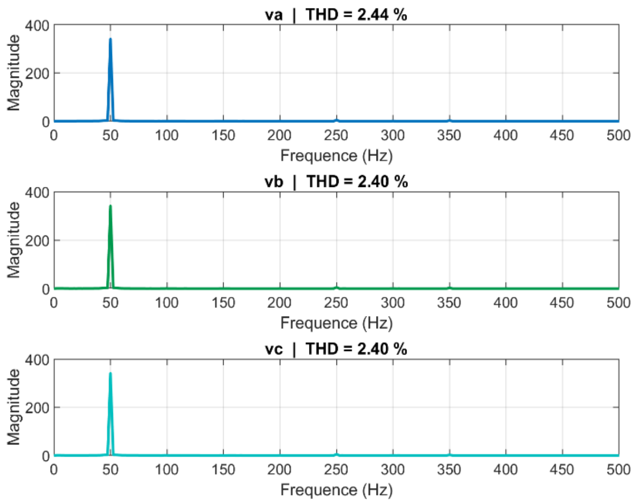

Fig. 26. Frequency analysis of the voltages va,vb and vc

V. Conclusion and future work

Furthermore, the DC-bus voltage is stably regulated around 1000 V despite variations in solar irradiance and load conditions. The batteries storage system plays a key role in energy balancing through the batteries charging and discharging operation according to production and consumption conditions. The observed power flows confirm an efficient distribution of energy between the PV, the batteries, and the load.

The three-phase inverter, controlled using the SVPWM technique and combined with an LC filter at its output, enables the generation of balanced and sinusoidal three-phase voltages and currents. The obtained results show a strong agreement between the reference signals and the actual quantities, as well as a good power balance. Frequency analysis highlights a low total harmonic distortion (THD) of 2.44% for both voltages and currents, confirming the high quality of the energy supplied to the micro-grid. This performance is mainly attributed to the effectiveness of the SVPWM strategy and the proper design of the LC filter.

The simulations are done under realistic conditions, demonstrate the relevance of the proposed strategy. The system ensures high power quality (low THD), stable operation, and optimized energy management, making it particularly suitable for stand-alone micro-grid applications in rural areas.

Acknowledgment

This work is done at the GREAH laboratory, Université Le Havre Normandie, France, by the Renewable Energies and Storage Systems (MERS) research team, as part of the 1000PhD and 5000 Masters train-the-trainer project initiated by the Ministry of Higher Education, Scientific Research and Innovation of the Republic of Guinea (MESRSI-GUINEE). The authors would like to thank the Guinean authorities for their financial support, and the University of Le Havre Normandie for the research activity support to ensuring the success of this project.

References

[1] M. L. Touré, M.-B. Camara, C. B. Nzoundja Fapi, A. Payman, and B. Dakyo, Eds., “Energy Management of PV-Batteries System for a Rural Micro-Grid Application in Guinea,” presented at the International Conference on Green Communications, Computing and Technologies, Wilmington, DE, USA: IARIA, 2025.

[2] A. Chellakhi and S. El Beid, “A Real-Time Investigation of an Enhanced Variable Step PO MPPT Controller for Photovoltaic Systems Using dSPACE 1104 Board,” *Energies*, vol. 18, no. 13, p. 3343, Jun. 2025, doi: 10.3390/en18133343.

[3] M. L. Touré, M. B. Camara, and B. Dakyo, “Symmetrical Multilevel High Voltage-Gain Boost Converter Control Strategy for Photovoltaic Systems Applications,” *Electronics*, vol. 13, no. 13, p. 2565, Jun. 2024, doi: 10.3390/electronics13132565.

[4] C. B. Nzoundja Fapi *et al.*, “Fuzzy Logic-Based Maximum Power Point Tracking Control for Photovoltaic Systems: A Review and Experimental Applications,” *Arch Computat Methods Eng*, vol. 32, no. 4, pp. 2405–2428, May 2025, doi: 10.1007/s11831-024-10210-7.

[5] C. H. Swetha, N. S. Jayalakshmi, K. M. Bhargavi and P. B. Nempu, “Control strategies for power management of PV/battery system with electric vehicle,” *In 2019 IEEE International Conference on Distributed Computing, VLSI, Electrical Circuits and Robotics (DISCOVER) (pp. 1-6). IEEE.*

[6] I. Oukkacha; M. B. Camara and B. Dakyo, “Energy Management in Electric Vehicle based on Frequency sharing approach, using Fuel cells, Lithium batteries and Supercapacitors,” *in Inter. Conf. on Renewable Energy Research and Applications (ICRERA2018), Paris, France, (pp. 986-992), IEEE.*

[7] M. O. Badawy and Y. Sozer, “Power flow management of a grid tied PV-battery system for electric vehicles charging”, IEEE Transactions on Industry Applications,” vol. 53, no. 2, pp. 1347–1357, 2017.

[8] A. Baqar, M. B. Camara, and B. Dakyo, “Supercapacitors Fast Ageing Control in Residential Microgrid Based Photovoltaic/Fuel Cell/Electric Vehicle Charging Station,” *Energies*, vol. 16, no. 13, p. 5084, Jun. 2023, doi: 10.3390/en16135084.

[9] M. P. Bonkile and V. Ramadesigan, “Power management control strategy using physics-based battery models in standalone PV-battery hybrid systems,” *Journal of Energy Storage*, vol. 23, pp. 258–268, Jun. 2019, doi: 10.1016/j.est.2019.03.016.

[10] S. Ahmad, M. Shafiullah, C. B. Ahmed, and M. Alowaifeer, “A Review of Microgrid Energy Management and Control Strategies,” *IEEE Access*, vol. 11, pp. 21729–21757, 2023, doi: 10.1109/access.2023.3248511.

[11] J. Hu, Y. Shan, K. W. Cheng and S. Islam, "Overview of power converter control in microgrids—Challenges, advances, and future trends", IEEE Transactions on Power Electronics," vol. 37, no. 8, p. pp. 9907–9922, 2022.

[12] S. J. Yaqoob, H. Arnoos, M. A. Qasim, E. B. Agyekum, A. Alzahrani, and S. Kamel, "An optimal energy management strategy for a photovoltaic/li-ion battery power system for DC microgrid application," *Front. Energy Res.*, vol. 10, Jan. 2023, doi: 10.3389/fenrg.2022.1066231.

[13] Y. Alidrissi, R. Ouladsine, A. Elmouatamid, and M. Bakhouya, "An Energy Management Strategy for DC Microgrids with PV/Battery Systems," *J. Electr. Eng. Technol.*, vol. 16, no. 3, pp. 1285–1296, May 2021, doi: 10.1007/s42835-021-00675-y.

[14] M. Benzaouia, A. Rabhi, B. Hajji, S. Benzaouia, H. Midavaine, and B. K. Oubbati, "Real-Time Control and Power Management Strategies of PV/Battery Standalone System," *IFAC-PapersOnLine*, vol. 56, no. 2, pp. 9135–9140, 2023, doi: 10.1016/j.ifacol.2023.10.151.

[15] C. B. Nzoundja Fapi, M. L. Touré, M.-B. Camara, and B. Dakyo, "Control Strategy for DC Micro-Grids in Heat Pump Applications with Renewable Integration," *Electronics*, vol. 14, no. 1, p. 150, Jan. 2025, doi: 10.3390/electronics14010150.

[16] S. R. Fahim, H. M. Hasanien, R. A. Turky, S. H. E. A. Aleem, and M. Ćalasan, "A Comprehensive Review of Photovoltaic Modules Models and Algorithms Used in Parameter Extraction," *Energies*, vol. 15, no. 23, p. 8941, Nov. 2022, doi: 10.3390/en15238941.

[17] M. B. Camara, H. Gualous, F. Gustin, A. Berthon, and B. Dakyo, "DC/DC Converter Design for Supercapacitor and Battery Power Management in Hybrid Vehicle Applications—Polynomial Control Strategy," *IEEE Trans. Ind. Electron.*, vol. 57, no. 2, pp. 587–597, Feb. 2010, doi: 10.1109/tie.2009.2025283.

[18] H. Rezk, A. M. Nassef, M. A. Abdelkareem, A. H. Alami, and A. Fathy, "Comparison among various energy management strategies for reducing hydrogen consumption in a hybrid fuel cell/supercapacitor/battery system," *International Journal of Hydrogen Energy*, vol. 46, no. 8, pp. 6110–6126, Jan. 2021, doi: 10.1016/j.ijhydene.2019.11.195.

[19] B. Benlahbib *et al.*, "Experimental investigation of power management and control of a PV/wind/fuel cell/battery hybrid energy system microgrid," *International Journal of Hydrogen Energy*, vol. 45, no. 53, pp. 29110–29122, Oct. 2020, doi: 10.1016/j.ijhydene.2020.07.251.

[20] M. A. Danandeh and S. M. Mousavi G., "Comparative and comprehensive review of maximum power point tracking methods for PV cells," *Renewable and Sustainable Energy Reviews*, vol. 82, pp. 2743–2767, Feb. 2018, doi: 10.1016/j.rser.2017.10.009.

[21] M. L. Katche, A. B. Makokha, S. O. Zachary, and M. S. Adaramola, "A Comprehensive Review of Maximum Power Point Tracking (MPPT) Techniques Used in Solar PV Systems," *Energies*, vol. 16, no. 5, p. 2206, Feb. 2023, doi: 10.3390/en16052206.

[22] R. Subbulakshmy and R. Palanisamy, "SVPWM control strategy for Novel Interleaved High Gain DC converter fed 3-level NPC Inverter for Renewable Energy Applications," *ISA Transactions*, vol. 140, pp. 426–437, Sep. 2023, doi: 10.1016/j.isatra.2023.05.019.

[23] S. Prajapati, R. Garg, and P. Mahajan, "Modified control approach for MPP tracking and DC bus voltage regulation in a hybrid standalone microgrid," *Electric Power Systems Research*, vol. 236, p. 110935, Nov. 2024, doi: 10.1016/j.epsr.2024.110935.

[24] I. Al-Wesabi, Z. Fang, H. M. Hussein Farh, A. A. Al-Shamma'a, and A. M. Al-Shaalan, "Comprehensive comparisons of improved incremental conductance with the state-of-the-art MPPT Techniques for extracting global peak and regulating dc-link voltage," *Energy Reports*, vol. 11, pp. 1590–1610, Jun. 2024, doi: 10.1016/j.egyr.2024.01.020.

[25] K. Boutaghane, N. Bennecib, M. Benidir, H. Benbouhenni, and I. Colak, "Performance enhancement of a three-phase grid-connected PV inverter system using fractional-order integral sliding mode controls," *Energy Reports*, vol. 11, pp. 3976–3994, Jun. 2024, doi: 10.1016/j.egyr.2024.03.049.

[26] A. Azizi, M. Akhbari, S. Danyali, Z. Tohidinejad, and M. Shirkhani, "A review on topology and control strategies of high-power inverters in large- scale photovoltaic power plants," *Heliyon*, vol. 11, no. 3, p. e42334, Feb. 2025, doi: 10.1016/j.heliyon.2025.e42334.